Tellus
SERIES B
CHEMICAL
AND PHYSICAL
METEOROLOGY
PUBLISHED BY THE INTERNATIONAL METEOROLOGICAL INSTITUTE IN STOCKHOLM

Tellus (2009), 61B, 195–205
Printed in Singapore. All rights reserved

TELLUS

Vertically resolved dust optical properties during SAMUM: Tinfou compared to Ouarzazate

By BIRGIT HEESE[1,2]*, DIETRICH ALTHAUSEN[1], TILMAN DINTER[3], MICHAEL ESSELBORN[4], THOMAS MÜLLER[1], MATTHIAS TESCHE[1] and MATTHIAS WIEGNER[2], [1]*Leibniz Institute for Tropospheric Research (IfT), Permoserstr. 15., 04318 Leipzig, Germany;* [2]*Meteorological Institute, Ludwig-Maximilians-Universität, Theresienstr 35, 80333 Munich, Germany;* [3]*Institute for Environmental Research, University of Bremen, Otto-Hahn-Allee 1, 28359 Bremen, Germany;* [4]*Deutsches Zentrum für Luft– und Raumfahrt, Institute for Atmospheric Physics, 82234 Wessling, Germany*

(Manuscript received 9 July 2008, in final form 30 October 2008)

ABSTRACT

Vertical profiles of dust key optical properties are presented from measurements during the Saharan Mineral Dust Experiment (SAMUM) by Raman and depolarization lidar at two ground-based sites and by airborne high spectral resolution lidar. One of the sites, Tinfou, is located close to the border of the Sahara in Southern Morocco and was the main in situ site during SAMUM. The other site was Ouarzazate airport, the main lidar site. From the lidar measurements the spatial distribution of the dust between Tinfou and Ouarzazate was derived for 1 d. The retrieved profiles of backscatter and extinction coefficients and particle depolarization ratios show comparable dust optical properties, a similar vertical structure of the dust layer, and a height of about 4 km asl at both sites. The airborne cross-section of the extinction coefficient at the two sites confirms the low variability in dust properties. Although the general picture of the dust layer was similar, the lidar measurements reveal a higher dust load closer to the dust source. Nevertheless, the observed intensive optical properties were the same. These results indicate that the lidar measurements at two sites close to the dust source are both representative for the SAMUM dust conditions.

1. Introduction

The radiative impact of mineral dust particles – one of the main uncertainties in climate forcing – is strongly controlled by their optical properties and their spatial distribution (Sokolik et al., 2001). One of the main sources for mineral dust is the North African desert, the Sahara. Saharan dust has been studied when transported over short ranges to Europe (e.g. Hamonou et al., 1999; Mattis et al., 2002; Ansmann et al., 2003; Balis et al., 2004) or over long ranges to the Caribbean Sea (e.g. Prospero and Carlson, 1972; Prospero et al., 1981, 1999; Reid et al., 2003) and also during various field campaigns over North Africa. Most recently, the Saharan Dust Experiment (SHADE; Tanré et al., 2003) in 2000, the Southern African Regional Science Initiative (SAFARI–2000), also in 2000 (Haywood et al., 2003), and the African Monsoon Multidisciplinary Analyses (AMMA; Redelsperger et al., 2006), in 2006, have been carried out. In most cases the dust was mixed with aerosol types of biomass burning or urban origin. During the SHADE campaign airborne lidar measurements allowed a characterization of mineral dust particles (Léon et al., 2003) between Dakar (Senegal) and Cape Verde Islands. Biomass burning aerosol has been characterized during the SAFARI–2000 campaign in Southern Africa. During the AMMA dry season special observation period in January 2006 Saharan dust and biomass burning particles were characterized by lidar profiling south of the Sahara (Chazette et al., 2007; Heese and Wiegner, 2008; Johnson et al., 2008) and were observed by aircraft in situ measurements (Osborne et al., 2008). Mineral dust was mainly present in the lowermost 2 km while biomass burning aerosol mixed with varying amounts of dust was observed in elevated layers up to 5 km. But pure dust conditions have rarely been met during those field experiments. To assure that pure dust is probed one has to place the instruments as close as possible to a source of mineral dust, that is, the Saharan desert (Sokolik et al., 2001).

This was the subject of the Saharan Mineral Dust Experiment (SAMUM): to characterize mineral dust particles close to their source and to quantify their radiative effects (Heintzenberg, 2008). The first field campaign was carried out in May and June 2006 in Southern Morocco to assure

*Corresponding author.
e-mail: heese@tropos.de
DOI: 10.1111/j.1600-0889.2008.00404.x

measurements of pure, not aged dust. Two field sites were chosen for the ground-based measurements. One of the sites was located at Tinfou, close to the town Zagora. Tinfou is one of the last posts before the Saharan desert in Morocco and offers almost pure dust conditions. It was the main site for in situ measurements of optical, microphysical and mineralogical properties of Saharan dust particles. The other site was Ouarzazate airport that lies about 100 km to the northwest in the Anti-Atlas Mountains where a small research aircraft for radiative and in situ measurements was deployed. A map showing these locations can be found in the introductory paper (Heintzenberg, 2008) and is shown by several other companion papers (e.g. Kahn et al., 2008; Kandler et al., 2008; Knippertz et al., 2008). Due to logistical reasons, all ground-based lidar systems were operated from Ouarzazate. These systems were three Raman and backscatter lidars of different sizes operating at different numbers of wavelengths and covering different measurement ranges. Thus, these lidars were complementing one another so that the dust optical properties of interest could be studied comprehensively at different wavelengths and ranges.

Due to financial limitations, no additional lidar could be installed at Tinfou. To have at least a few examples of the vertical distribution of the dust and its diurnal variation, one of the lidars the small, portable Raman lidar system (POLIS) was moved from Ouarzazate to Tinfou for a short stay. The measurements at Tinfou allow to investigate if the distance to Ouarzazate and the orographic differences between the two sites has an impact on the results obtained at Ouarzazate. Are the dust particles probed at both sites of the same type? And thus, is it possible to combine the results from both sites for the vertical closure study that SAMUM aimed at? Or have the mineral particles already undergone a significant change in any of their optical properties?

To study the regional variability of the dust layer we compare simultaneous lidar profiles of dust optical properties at both sites and connect them with a corresponding airborne lidar cross-section. In Section 2, we introduce the SAMUM field campaign and present the instruments used in this study. In Section 3, the lidar evaluation methods are described and in Section 4, the results of our case study are presented and discussed. Section 5 gives a short summary and conclusion.

2. Field campaign and instrumentation

2.1. Tinfou

The vertical probing of desert dust optical properties presented in this paper took place at Tinfou. The site is located on the property of the Hotel Porte au Sahara (30.2°N, 5.6°W) 30 km southeast of Zagora, Morocco, at the border of the Saharan desert. This remote place was the main SAMUM site for in situ measurements of the Saharan dust properties because it has two main advantages: it is close to the desert without disturbing settlements in-between, so that pure dust conditions were expected there. The site is easily accessible by car so that mid-size equipment – as the small, portable lidar POLIS – can be transported there. The altitude is 680 m above sea level (asl). Lidar measurements at Tinfou were conducted on 3 d from the evening of 26 May to mid-day of 28 May 2006.

The lidar used for the measurements in Tinfou was the portable Raman and polarization lidar POLIS which was developed at the Meteorological Institute at the University of Munich. POLIS is a small, rugged, two channel lidar. It emits pulses of linear polarized light at the wavelength of 355 nm. By choosing the wavelength in the ultraviolet region, where the eye is less sensitive, the lidar is eye-safe beyond a distance of 30 m from the laser. Two detection channels are available and the data acquisition allows a vertical sampling with 7.5 m resolution. The laser is mounted directly onto the receiving telescope to minimize the distance between the laser axis and the telescope axis. As a consequence the overlap between the emitting and receiving fields of view of POLIS is completed at 120 m. More technical details of this lidar system are described by Heese et al. (2002, 2004). POLIS can be operated in two modes: either in the depolarization mode or in the Raman mode. In the depolarization mode, the two channels of the lidar are used for measuring the parallel- and cross-polarized components of the backscattered light to determine the depolarization ratio at 355 nm. In the Raman mode, measurements at 355 nm and at the nitrogen Raman shifted wavelength at 387 nm are performed. Since two different detection units exist, one for depolarization and one for Raman measurements, switching between the measurement modes is easily done by replacing the complete detector block. Due to precise manufacturing of the mechanical components no optical re-alignment of the system is necessary.

The aerosol optical depth (AOD) measured by sun photometry is an optical property that can be used to evaluate lidar retrievals. At Tinfou a Cimel CE 318 sun photometer owned by the University of Bremen was operated during SAMUM. This sun photometer was equipped with additional channels in the ultraviolet at 341 and 379 nm and in the near infrared at 1020 nm. Measurements of the direct solar radiation and the angular and spectral sky radiance in the almucantar regime were performed regularly. The AOD was determined from the direct sun measurements at eight channels by the coupled inversion radiation transfer (CIRATRA; Wendisch et al., 1994; von Hoyningen-Huene et al., 1997) approach. This algorithm has been improved by an aureole correction for additional light in the instruments field of view for desert cases and is described by von Hoyningen-Huene et al. (2008). For the comparison with the lidar wavelength at 355 nm, the two additional channels in the ultraviolet are used.

To cover the lowermost heights, where the overlap of the lidars emitter and receiver is not complete yet, extinction data from a visibility meter was used. The visibility meter (model VPF-710,

Biral, Bristol UK) was operated at Tinfou by IfT and measures the extinction coefficient at 880 nm. The principle operation is to measure the forward scattered light in a small undisturbed sample volume of about 400 cm^3 at a scattering angle of 45°. The scattered intensity is a direct measure of the extinction coefficient. The extrapolation from 880 to 355 nm was done using an Ångström coefficient of 0.2. This value coincides with the mean Ångström coefficient observed by the sun photometer in Tinfou.

2.2. Ouarzazate

While POLIS was in Tinfou the two other SAMUM lidar systems were continuing measurements at Ouarzazate airport (30.9°N, 6.9°W]. The airport lies at 1133 m asl between the high Atlas Mountain ridge to the northwest and the lower Anti-Atlas to the southeast. Those two lidars were the mobile, scanning multiwavelength lidar MULIS of the University of Munich and the six-wavelength backscatter extinction lidar-ratio temperature humidity profiling apparatus (BERTHA) of the IfT (Althausen et al., 2000). MULIS is emitting the three Nd:YAG laser wavelengths 355, 532 and 1064 nm and has six receiving channels including two nitrogen Raman channels at 387, 607 nm and a depolarization channel at 532 nm. More details of this lidar system and an analysis of dust depolarization properties during SAMUM are described by Freudenthaler et al. (2008). The six wavelengths emitted by BERTHA are 355, 400, 532, 710, 800 and 1064 nm. In this study, the extinction profiles derived at the ultraviolet and the visible wavelengths are used. BERTHA is a scanning lidar system. During daytime measurements were conducted at the elevation angle of 45° and – to avoid specular reflections from cirrus clouds (Platt, 1978) – at an angle of 5° off the zenith during nighttime. A comprehensive analysis of BERTHA data is given by Tesche et al. (2008).

For the measurements of the AOD at Ouarzazate the Aerosol Robotic Network (AERONET; Holben et al., 1998) sun photometer of the Leipzig lidar group was deployed. It is equipped with an additional long wavelength channel at 1640 nm for improved dust observations. The AERONET sun -photometer measures direct sunlight at eight channels: 339, 379, 441, 501, 675, 869, 940, 1021 and 1638 nm wavelength. The AOD data used in this study are quality assured AERONET retrievals.

2.3. Aircraft

Finally, the DLR Falcon-20 research aircraft was deployed at the airport of Casablanca. Onboard, besides numerous particle collecting and in situ experiments, a high spectral resolution lidar (HSRL; Esselborn et al., 2008) was operated during SAMUM. Several overflights over the ground-based sites gave the opportunity of intercomparisons between airborne and ground-based lidar profiles and allow to study the spatial distribution of the dust.

3. Evaluation of POLIS data

The optical properties measured by aerosol lidar are depolarization ratio, particle backscatter and extinction coefficients and lidar ratio. Depolarization is a parameter that depends on the shape of the particles. Extinction coefficient depends on scattering and absorbing properties of the particles but also on the number and size distribution of the particles. This is also valid for the vertically integrated extinction, the optical depth. Finally, the extinction-to-backscatter ratio, the lidar ratio, is again characteristic for the various particle types.

In the following subsections, the derivation of these optical properties from the lidar data is explained in more detail.

3.1. Depolarization ratio

The depolarization ratio characterizes atmospheric particles and identifies aspherical particles as, for example, mineral dust particles or cirrus clouds. Two types of depolarization can be determined from the lidar signal: the total or volume depolarization and the particle depolarization.

The volume depolarization is the direct ratio of the backscatter signal received in the plane that is cross-polarized to the laser's polarization to the signal received in the plane parallel to it. It can be derived with a high temporal resolution of 30 s. The volume depolarization comprises the relative contribution of particles and air molecules in terms of backscatter coefficients. For an accurate retrieval the relative sensitivity of the two channels against each other has been determined. This is done by a calibration of the channels by rotating the polarizing beam splitter cube by 45° in both directions from its normal position. At these positions the polarizing beam splitter cube transmits both polarization planes of the incoming light equally. From the ratio of these signals the relative sensitivities of the channels can be determined. A calibration using both rotations minimizes the error in positioning the polarizing beam splitter cube.

To get a measure only depending on particle properties, the particle depolarization ratio must be calculated. The particle depolarization is an intensive optical property that characterizes the particles itself in composition and shape and is independent of the number of observed particles. For this purpose, the volume depolarization must be converted into particle depolarization using the corresponding molecular and particle backscatter coefficients (e.g. Cairo et al., 1999; Murayama et al., 1999). To calculate the molecular backscatter coefficient radio soundings performed at Ouarzazate airport were used. The particle backscatter profiles are derived from the lidar measurements.

3.2. Backscatter and extinction coefficient and lidar ratio

An extensive aerosol optical property derived from lidar measurements is the particle extinction coefficient. An extensive

optical property depends not only on the particles composition and shape but increases with the number of observed particles. Particle extinction is one of the key input parameters for radiative transfer calculations. It can be derived from lidar signals in two ways: either from the elastic signal at the emitted laser wavelength, which is 355 nm in the case of POLIS, or from the inelastic Raman signal at 387 nm.

From the inelastic Raman signal the direct determination of the particle extinction coefficient without a priori assumptions is possible (Ansmann et al., 1992). This is due to the fact that the Raman signal at 387 nm scattered back by nitrogen molecules is only affected by particle extinction and known optical properties of the air molecules. From the Raman signal and the corresponding elastic signal at 355 nm the backscatter coefficient and thus the backscatter-to-extinction ratio, the lidar ratio, can be derived. The lidar ratio is again an intensive optical property that is specific for the observed particle type and does not depend on the number of particles. The nighttime Raman measurements are averaged over at least 1 h to achieve an extinction profile up to the upper troposphere with an error of less than 25%. Due to the relatively low Raman signal compared to the sky background during daytime Raman measurements are restricted to nighttime.

During daytime the retrieval of the extinction coefficient from the elastic signal is done by the method described by Fernald (1984) assuming a realistic value for the lidar ratio, to solve the underdetermined lidar equation. This lidar ratio can be derived from nighttime Raman measurements. As will be shown later, the lidar ratio for dust inside the nighttime boundary layer was found to be 55 sr. This value coincides with lidar ratios observed earlier in dust layers. During AMMA the lidar ratio observed in the dust layer by POLIS was 55 ± 5 sr (Heese and Wiegner, 2008). And from an episode, when Saharan dust particles were transported towards Europe (Ansmann et al., 2003) the observed lidar ratio was 59 ± 11 sr. Also from the SAMUM lidar measurements at Ouarzazate the lidar ratio of dust particles was determined as 55 ± 6 sr (Müller et al., 2007; Tesche et al., 2008). Thus, a mean lidar ratio of 55 sr was applied to derive the particle extinction by the Fernald method for all daytime measurements from POLIS during SAMUM.

3.3. Aerosol optical depth

Aerosol optical depth can be derived from the lidar measurements by vertical integration of the extinction coefficient profile. The profiles are integrated from the lowermost lidar height up to a height well above the dust layer, which was chosen at 7.5 km asl. In the absence of clouds, above this height no contribution to the AOD needs to be added. This is justified by the fact that in all retrieved lidar profiles the extinction coefficients are below 0.01 above the dust layer. One exception is a 15 min period on 28 May 2006 where a thin cirrus was observed at 11 km height. The contribution of this cirrus to the AOD is discussed by Kahn et al. (2008). Close to the ground the extinction coefficient is extrapolated to a ground-level extinction value measured by the visibility meter. Finally, the resulting AOD is compared to the AOD obtained from sun photometer measurements at the wavelength 341 and 379 nm and interpolated to the lidar wavelength at 355 nm.

4. Lidar profiles

On 26 May 2006 POLIS was transported to the site at Tinfou to stay there until 28 May 2006. Raman lidar measurements were performed on the evenings and depolarization measurements were performed during daytime. After about noon the measurements have been stopped because air temperatures exceeded 35°C and the water cooling circuit of the laser became too weak.

In the following, we present examples of Raman and Fernald derived backscatter and extinction coefficients, corresponding lidar ratios and the particle depolarization observed inside the dust layer. From the high temporal resolution volume depolarization data the monitoring of the mostly undisturbed development of the dust layer is shown during one morning. To determine the spatial distribution of the dust a case study was conducted on 28 May 2006. The lidar profiles measured in Tinfou are compared to measurements performed at Ouarzazate and interpreted in conjunction with the airborne HSRL profiles from a Falcon overflight over both sites. These profiles are then related to the dust distribution observed during SAMUM at Ouarzazate and during the POLIS measurement period at Tinfou.

4.1. Raman measurements and lidar ratio

Extinction coefficient profiles and extinction-to-backscatter or lidar ratio were derived from POLIS Raman measurements taken in the late evenings. On 26 May 2006 a significant fraction of dust has been washed out by heavy rain showers in the afternoon. On 27 May 2006 the dust layer has recovered quickly. The extinction coefficient profiles, backscatter profiles and lidar ratios derived from the Raman measurement are shown in Fig. 1. The extinction and backscatter profiles show a well-developed dust layer that reaches up to approximately 4.3 km. The lidar ratio resulting from these measurements is quite constant inside the dust layer and the mean value is 55 ± 8 sr. For comparison, the backscatter and extinction profiles retrieved from the same raw signal using the Fernald method with the constant lidar ratio of 55 sr are plotted. The agreement of the profiles is very good: the same structure of the dust layer is resolved as by the Raman measurement, especially in the backscatter profile. The differences in the upper part of the extinction profile is due to different height averagings. This comprises an increasing height interval with altitude for the Raman measurements to account for the decreasing signal-to-noise ratio with altitude: At 1 km altitude the Raman signal is derived with vertical smoothing with a window

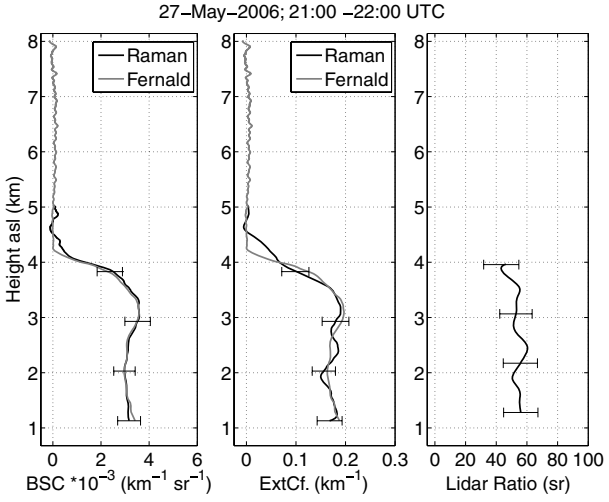

Fig. 1. Backscatter and extinction coefficients derived from Raman measurements compared to Fernald retrievals and resulting lidar ratio for Saharan dust particles at Tinfou on 27 May 2006. The error of the Raman derived backscatter coefficient results from signal–noise in the order of 10% and a systematic error due to Rayleigh scattering correction and signal calibration estimated to about 5%. The error of the Raman extinction coefficient is in the same order. The lidar-ratio error results form these two errors by error propagation.

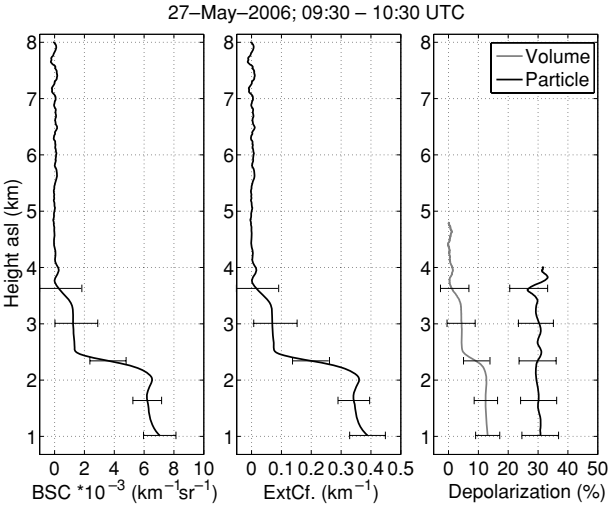

Fig. 2. Backscatter and extinction coefficients derived with the Fernald method using a lidar ratio of 55 sr and depolarization ratio, measured at Tinfou on 27 May 2006. Note the different scales of the abscissae for the backscatter and extinction profiles compared to the other figures. The error of the backscatter coefficient comprises 10% due to signal–noise and an estimated systematic error of 10% due to Rayleigh scattering. Because the lidar ratio is well known from the Raman measurements the relative error of the extinction coefficient equals the relative error of the backscatter coefficient. The error of the volume and particle depolarization ratio is about 15% and 20%, respectively. Besides signal–noise the main contributions to these errors result from the depolarization calibration and, in case of the particle depolarization, from the errors in molecular and particle backscatter.

lengths of 400 m, at 2 km of 600 m and at 4 km of 1 km. The profiles by the Fernald method are vertically smoothed over a constant height interval of 300 m.

The extinction coefficient profile shows values up to 0.2 km^{-1} throughout the whole dust layer. The AOD integrated from this extinction profile is 0.52, which is close to the AOD of 0.55 measured by the sun photometer in the evening just before sunset. The AOD measured by the sun photometer did decrease from around 1 in the morning to around 0.5 in the course of this day. These values are fully comparable to dust extinction coefficient measured earlier. For example, during AMMA the mean extinction coefficients for dust measured by POLIS in the Sahel region were around 0.2 km^{-1}. For 1 d with direct import of dust loaded air masses from the Saharan desert, the extinction coefficient could exceed 1.5 km^{-1}. However, the vertical extent of this layer was only a few 10 m (Heese and Wiegner, 2008). Extinction values in the same order are presented by Johnson et al. (2008), who show airborne nephelometer measurements compared to airborne lidar measurements (Chazette et al., 2007) with ground-based measurements from POLIS and an MPL lidar stationed at Niamey Airport. Further south in Benin a microlidar also measured extinction coefficient in the order of 0.2 km^{-1} in the dust layer close to the ground (Pelon et al., 2008).

4.2. Daytime extinction coefficients

During daytime, when the sky background is too high for the weak Raman signal depolarization ratio measurements were performed. The extinction and backscatter profiles were derived from the total lidar signal by combining both depolarization channels. The profiles were calculated using the Fernald method with a lidar ratio of 55 sr, as determined from the nighttime Raman measurements. Fig. 2 shows a two-layer structure of dust on 27 May. The upper boundary of the dust layer on this day is at around 3.8 km. The extinction coefficient in the lower part of the newly developing dust layer is reaching values of 0.4 km^{-1}. Above this layer the residual layer from the night before is still present. Here the extinction values are around 0.08 km^{-1}. At ground level the extinction coefficient measured by the visibility meter is between 0.68 km^{-1} at 10:00 UTC and 0.54 km^{-1} at 10:30 UTC. The integration of the lidar profile and extrapolation to the ground values gives an AOD of 0.75, which is in good agreement with the values measured by the sun photometer of around 0.79 at 10:00 UTC. This difference in AOD is only about 5 %, which is inside the uncertainty of the extinction coefficient imposed by the lidar-ratio error. Thus, we can conclude that the mean lidar ratio from the night is also valid for the morning hours. The comparably high value of the AOD was caused by high surface winds. Around 10:00 UTC the surface wind speed was rising up to 10 ms^{-1}, and dust from local sources was mobilized and mixed into the lower boundary layer.

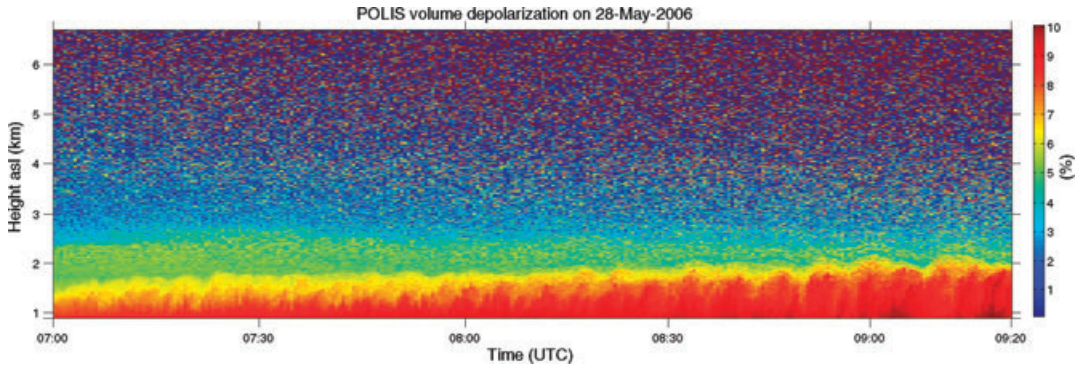

Fig. 3. High resolution volume depolarization measured at Tinfou from 7:00 to 9:20 UTC on 28 May 2006, showing the development of the diurnal dust layer in the early morning hours. The residual layer up to 4 km (see next figure) with very low volume depolarization ratios cannot be resolved with 30 s time resolution.

4.3. Depolarization

Despite the two layers observed in the extinction and backscatter profiles, on 27 May the particle depolarization ratio throughout the whole boundary layer is constant and has a value of 30% ± 6% (see Fig. 2, right-hand panel). This value was also measured the next day and is shown in Fig. 4 (right-hand panel). Here high particle depolarization ratios with values between 26% and 36% throughout the dust layer were observed. Since the particle depolarization is an intensive optical property these measurements imply that the particles in the dust layer and in the residual layer above are of the same type. Observations in Ouarzazate from all lidar systems show that these values are representative for the dust layer close to the source region. Freudenthaler et al. (2008) have studied the depolarization ratio at four wavelengths (355, 532, 710 and 1064 nm) and found very low wavelength dependence of the depolarization and mean values around 30% during dust episodes.

To visualize the temporal development of the dust layer during the day the high resolution volume depolarization measurements are very useful. On 28 May 2006 the measurements started early in the morning (Fig. 3). This was done to achieve a long measurement series in parallel with co-located sun photometer measurements by the University of Bremen. Two layers can be identified: The lowermost layer with the highest volume depolarization ratio with values of up to 10% – shown in red and yellow colours – has reached a height of about 1.2 km asl at 7:00 UTC which corresponds to 500 m above ground level (agl). The dust layer extends with the solar elevation and its upper boundary is already at about 2 km at 9:20 UTC. Note the wave-like structure of the upper boundary caused by turbulent mixing. The size of the eddies can be approximated from their vertical extent, which reached about 1 km above ground around 9:00 UTC and is growing on over the course of the day. Above this newly developing dust layer a residual layer with volume depolarization ratios around 5% can be identified up to a height of approximately 2.5 km asl. The upper boundary of the residual layer is stable throughout the morning. That the depolarization ratio is a good tracer for boundary layer dynamics has been shown previously by Gibert et al. (2007).

4.4. Dust distribution between Tinfou and Ouarzazate

The aim of this study is to find out if the choice of two different sites for the SAMUM field campaign is valid in terms of comparable retrieved dust optical properties. For this the lidar profiles measured at Tinfou shall be compared to those measured at Ouarzazate. Unfortunately, due to heavy rain on 26 May and some rain showers and cloudiness on 27 May, no lidar measurements were possible at Ouarzazate. But finally the intercomparison could be performed on 28 May, when POLIS was still operating at Tinfou and the two other SAMUM lidars were again measuring at Ouarzazate. An additional advantage on this day is that an overflight over both sites with the DLR Falcon was conducted. Onboard the HSRL was measuring backscatter and extinction profiles at the wavelength 532 nm and the backscatter coefficient at 1064 nm. One of the Falcons flight legs was crossing over Ouarzazate at 10:43 UTC and flew on directly to the other site at Tinfou where it arrived at 10:53 UTC. This case study also supports investigations on the spatial representativeness of the lidar measurements.

The corresponding backscatter and extinction profiles at 532 nm measured over Tinfou are plotted together with POLIS profiles of backscatter and extinction coefficients at 355 nm in Fig. 4 (left-hand and middle panel). The profiles from POLIS agree well with the HSRL profiles in shape and also in magnitude, especially at heights above 2 km. Below this altitude in the lower boundary the backscatter coefficient from the HSRL is higher but the extinction profiles are quite similar. These differences are due to different spatial coverages and a limited time averaging period by the aircraft. The measurement by the HSRL is spatially averaged over 30.37°–30.31°N and 5.72°–5.75°W, corresponding to a flight path of about 20 km and a time period from 10:53:22 to 10:54:06 UTC. The freshly raised dust particles in the lower boundary layer are subject to higher spatial

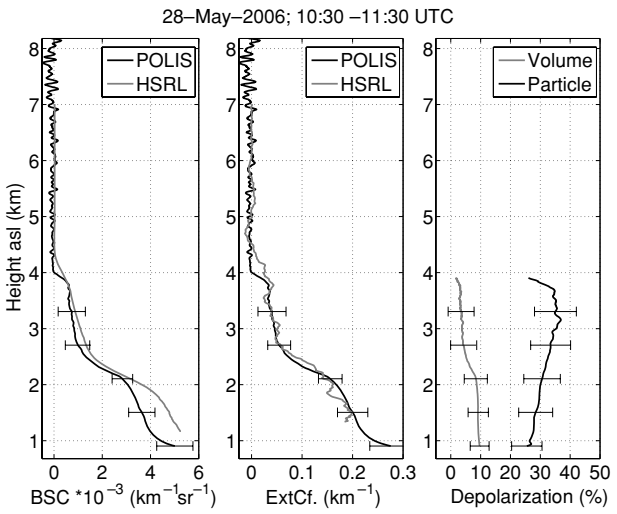

Fig. 4. Backscatter and extinction coefficients measured on 28 May 2006 by POLIS at 355 nm (derived with the Fernald method using a lidar ratio of 55 sr) and by the DLR Falcon high spectral resolution lidar (HSRL) at 532 nm during the Falcon overflight from 10:53:22 to 10:54:06 UTC, and POLIS volume and particle depolarization ratios at 355 nm at Tinfou. For error estimation see Fig. 2.

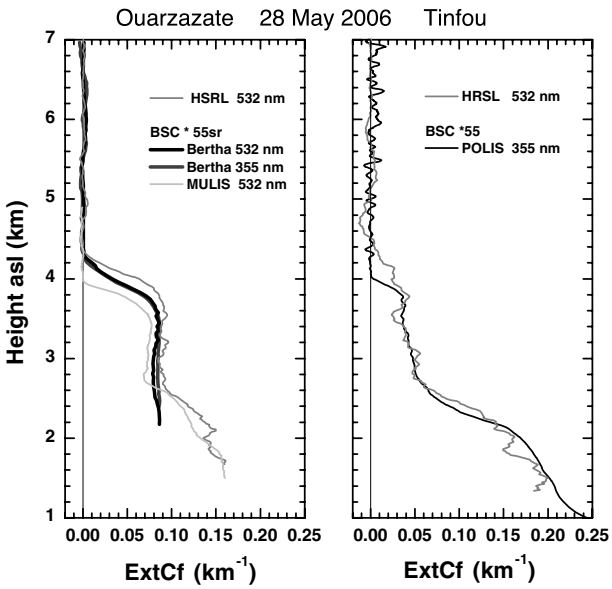

Fig. 5. Lidar extinction profiles measured on 28 May 2006, by BERTHA and MULIS at Ouarzazate from 09:53 to 11:34 UTC compared to the HSRL during the Falcon overflight at 10:42:44 - 10:44:10 UTC (left-hand side). Backscatter extinction lidar-ratio temperature humidity profiling apparatus measured with a zenith angle of 45°, MULIS at 88°, and HSRL was nadir looking. Note that the ground-based lidars have different geometrical factors (see Section 4.4). The errors of these measurements are discussed by Tesche et al. (2008) and Esselborn et al. (2008). On the right-hand side POLIS and HSRL extinction profiles at Tinfou during the overflight from Fig. 4 are displayed again for easy comparison.

variability than in the more settled residual layer from the night. In the present case the airborne measurements were averaged over a region that lies to the west of Tinfou where the dust concentration was slightly higher. This can be seen also in the upper panel of Fig. 6. The wavelength dependence of the backscatter coefficient is very low for dust particles. Therefore, the different wavelengths of the HSRL and POLIS signals should not contribute to the observed discrepancies.

This low wavelength dependance can be demonstrated by considering the measurements from a sun photometer. At Tinfou those measurements show that the columnar Ångström coefficient of the AOD is almost wavelength independent: it lies between 0 and 0.2 (von Hoyningen-Huene et al., 2008). This is also in agreement with the Ångström coefficient measured at Ouarzazate by the SAMUM lidar systems (Tesche et al., 2008), and with previous measurements of Saharan dust outbreaks observed over Europe (e.g. Mattis et al., 2002; Ansmann et al., 2003; Balis et al., 2004). However, parts of the observed differences may still due to different lines of vision of the two lidars. The differences in backscatter are also reflected in a differing lidar ratio at the lower altitudes. The mean lidar ratio derived from the backscatter and extinction profiles measured by the HSRL at the lower altitudes is around 38 ± 5 sr at 532 nm. As for all daytime measurements POLIS profiles at 355 nm were derived with the lidar ratio of 55 sr. To examine if this lidar ratio was also valid on this day, the resulting extinction profile was integrated to an AOD of 0.39. This AOD compares well with the value of 0.40 measured by the sun photometer at Tinfou. Since we do not see a significant difference in AOD we can assume that the extinction profile from POLIS derived by the Fernald method delivers reasonable results for this day.

The comparison of the profiles of extinction coefficients taken by MULIS and BERTHA at Ouarzazate during the Falcon overflight also coincides well with the profile from the airborne HSRL. Figure 5 (left-hand panel) shows the extinction profiles from BERTHA at 355 and 532 nm, and from MULIS and the HSRL at 532 nm (MULIS data were provided by V. Freudenthaler, Meteorological Institute at the University of Munich). For direct comparison the profiles observed at Tinfou are plotted again in Fig. 5 (right-hand panel). The profiles measured at Ouarzazate resemble in shape and magnitude to the profiles measured at Tinfou. A similar two-level dust layer is reaching up to altitudes around 4–4.2 km asl. The residual dust layer from the night is again present above 2.6 km and shows extinction values around 0.08 km^{-1}, compared to 0.06 km^{-1} at Tinfou. Below 2.6 km, inside the newly developed dust layer, the profiles from MULIS and the HSRL show extinction values of up to 0.15 km^{-1}, compared to 0.2 km^{-1} at Tinfou. The profiles from BERTHA are not shown below 2.2 km asl, because the overlap between laser and receiving telescope is not complete before 1.1 km above ground (see also Fig. 2, Tesche et al., 2008). The

ground-based lidars have all different geometrical factors. The smaller MULIS has a complete overlap at 250 m above ground. For comparison, POLIS overlap is already complete at 120 m above ground. Since the HSRL is measuring downward looking its profiles always reach the ground.

A disagreement in the profiles at Ouarzazate is a differing boundary layer top. It results mainly from different vertical resolutions and smoothings: BERTHA data are vertically smoothed over 660 m. The HSRL has a vertical resolution of 530 m. MULIS data were calculated from backscatter coefficients using the lidar ratio from the HSRL and are smoothed with a sliding average of 75 m. The larger smoothing window from BERTHA and HSRL leads to a less pronounced upper boundary than in the profile by MULIS. But also the averaging times and different spatial resolutions of the HSRL compared to the stationary measurement of the ground-based lidar are different. The HSRL profile was averaged from 30.9°–30.0°N and 6.9°–6.8°W which corresponds to a temporal average of 86 s. The ground-based measurements are averaged over about 1.5 h to achieve a low-noise lidar signal. But independently of the slightly differing observed boundary layer heights by the lidar systems the determined particle properties are still comparable.

Although the profiles from Ouarzazate and Tinfou only represent a snapshot of the dust optical properties during one morning these results imply that the spatial variability of the dust layer over the distance of 100 km between Tinfou and Ouarzazate is rather low. An overview over the dust optical properties measured by lidar at Ouarzazate is presented by Tesche et al. (2008): They conducted a height resolved statistical analysis that revealed a dust layer depth of typically 4–6 km height asl. A vertically inhomogeneous dust plume with internal dust layers was usually observed in the morning, before the evolution of the convective boundary layer. The Saharan dust layer was then well mixed in the early evening. The 500 nm dust optical depth ranged from 0.2 to 0.8 at Ouarzazate, Ångström exponents derived from photometer and lidar data were mainly between 0 and 0.4. The volume extinction coefficients varied from 0.03 to 0.3 km^{-1} with a mean value of 0.1 km^{-1} in the lowest 3 km agl. Mean extinction–to–backscatter ratios of 53–55 sr (±7–13 sr) were obtained at 355, 532 and 1064 nm. A significant wavelength dependence of the lidar ratio was not observed close to the source region of atmospheric desert dust. The values of the optical properties of the dust layer measured at Tinfou during the three lidar measurement days lay within these margins. The dust layer height at Tinfou was 4 km asl, the extinction coefficients in the dust layer were between 0.1 and 0.2 km^{-1}, and the AOD was around 0.4. During the whole SAMUM campaign the AOD at Tinfou was varying between 0.2 and 1.2 (von Hoyningen-Huene et al., 2008), slightly higher values than at Ouarzazate. But only a few days with a high AOD greater than 1 were observed and they were again caused by local dust activation when the wind speed was above 10 m s^{-1}. For most days the Ångström exponent is low (0.03–0.4). These results encourage us to conclude that we observe the same typical optical properties for pure dust at both sides.

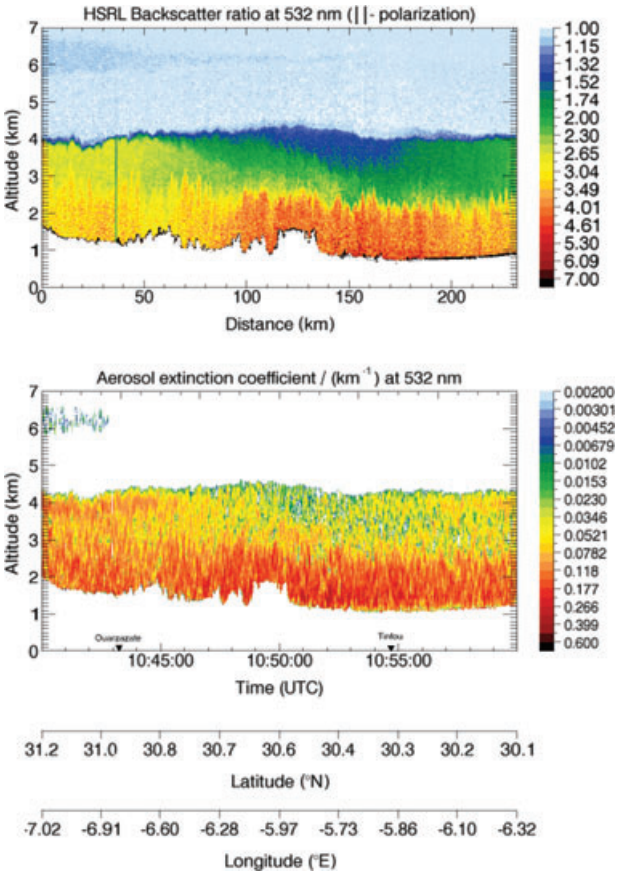

Fig. 6. Cross-section of airborne HSRL backscatter ratio and particle extinction coefficient during the Falcon flight over Ouarzazate and Tinfou on 28 May 2008. Altitudes are given in kilometre above sea level.

To further study the spatial variability of the dust layer cross-sections of backscatter ratio and extinction coefficient derived from the airborne lidar measurements are shown in Fig. 6. These cross-sections give a good overview over the dust distribution between Tinfou and Ouarzazate on 28 May 2006. This was a day of moderate dust load with AODs up to 0.5. The extinction values east of the mountain ridge at 30.6°N show the developing dust layer with the highest values up to 2.5 km a.s.l., the same structure as observed by POLIS over Tinfou. West of the mountains the dust load is decreasing and starts to disperse into the upper boundary layer. The lidar extinction profiles measured at Ouarzazate show values of about 0.05 km^{-1} lower than at Tinfou. This is consistent with the slightly lower dust load observed over Ouarzazate. The differing amount of dust is also reflected in the lower backscatter ratio west of the mountains. The AOD measured by sun photometry at Ouarzazate at 11:0 UTC was 0.35, compared to 0.39 at Tinfou.

HYSPLIT backtrajectories (Draxler and Rolph, 2003) ending at Tinfou and Ouarzazate on 28 May 2006 at 11 UTC (not shown) support the assumption that the same air masses were advected at both sites. The backtrajectory arriving at 1 km asl at both sites came from the southeast and originated from Algeria. The backtrajectories arriving at 2 and 3 km asl at both sites follow a cyclonic circulation from the south and southwest. The meteorological situation during the whole SAMUM campaign was intensively analysed by Knippertz et al. (2008) using backtrajectories. They show that several high dust and intermediate phases with lower dust impact did alternate during SAMUM. The high dust phases were dominated by air mass advection from the east and southeast, that is, northern and central Algeria. But also during the low dust phases advection from the east occurs, for example, in connection with a high pressure systems over the Atlas Mountains. 28 May was the last day of the second high dust phase of SAMUM. It was characterized by a cut-off low over northwestern Africa. The corresponding circulation is reflected in the mid-level HYSPLIT trajectories for both sites in our study. At lower levels there is still an easterly inflow of dust from Algeria, before the next intermediate low dust phase started later on that day. Due to the geographical location closer to Algeria, the dust load at these lower levels is higher at Tinfou than at Ouarzazate (see Fig. 5). From this trajectory analysis we can conclude that the same air mass accounts for the same structure of the dust layer observed over Tinfou and Ouarzazate on this day. From the common easterly advection of dust during the high dust phases we can conclude that in these cases comparable dust conditions were present at both sites and thus similar dust optical properties were observed.

5. Summary and conclusions

In this study, lidar profiles of dust backscatter and extinction coefficients and of volume and particle depolarization ratios are presented. The profiles were measured by several lidar systems in the frame of the first field campaign of the German SAMUM project in Southern Morocco. Lidar profiles at the two SAMUM ground sites, Tinfou and Ouarzazate, and from an airborne lidar were used for a case study of the spatial variability of the dust. The comparison of the derived particle properties at both sites show good agreement in particle depolarization, which lets us conclude that dust particles of the same type and shape were observed. The comparison also revealed excellent agreement in extinction coefficient with the profiles obtained from an airborne HSRL during the overpasses over the sites. However, the typical extinction coefficients and the resulting AODs were slightly higher in Tinfou compared to Ouarzazate. This is mainly due to more local dust sources and thus a higher amount of dust mixed into the boundary layer east of the Anti-Atlas Mountains. A similar structure and height of the dust layer was observed at both sites. During daytime the new dust layer is developing while the residual layer from the night is still present at higher altitudes. In the course of the day the dust layer height is raised by vertical mixing by convective processes like dust devils and convective dust plumes (see also Ansmann et al., 2008). In the evenings the lidar profiles show a well-mixed dust layer extending up to 4 km asl.

Though the time period of the POLIS measurement at Tinfou was limited and thus the comparison is not based on statistics we can conclude that there are no indications of significant differences in the mineral dust characteristics over a spatial scale of 100 km. During this comparison, the meteorological conditions were providing that the same dust layer was observable at both sites. The pure and fresh dust layer probed in Tinfou was essentially consisting of the same dust particle type that has been observed over Ouarzazate. This encourages us to assume that results found at one site are valid for the other site as well and both sites together can be used to describe dust particles close to their source region.

Certainly, dissimilarities in the dust layer occur due to regional orographic features. In the case of Ouarzazate and Tinfou, which are separated by the lower Anti-Atlas Mountains, these are minor differences. In contrast, the high Atlas Mountains west of Ouarzazate may cause a significant change in the optical properties by mixing marine aerosol with the dust particles (Esselborn et al., 2008). From this, we can conclude that although the dust load is higher closer to the desert, the observed two-layer structure of the dust layer is in principle the same, and, more important, the dust optical properties measured at both sites are comparable. Finally, we can conclude that Ouarzazate was close enough to the North African sources of mineral dust to allow the characterization of pure mineral dust particles by lidar profiling. The choice of the main lidar site at Ouarzazate airport – where the necessary logistical conditions for the big lidar systems were available – away from the in situ site was an appropriate alternative.

6. Acknowledgments

The SAMUM researcher group was funded by the German Science Foundation (DFG) under Grant FOR539.

The authors gratefully acknowledge the NOAA Air Resources Laboratory (ARL) for the provision of the HYSPLIT transport and dispersion model used in this publication.

References

Althausen, D., Müller, D., Ansmann, A., Wandinger, U., Hube, H. and co-authors. 2000. Scanning 6-wavelength 11-channel aerosol lidar. *J. Atmos. Ocean. Technol.* **17**, 1469–1482.

Ansmann A., Wandinger, U., Riebesell, M., Weitkamp, C. and Michaelis, W. 1992. Independent measurement of extinction and backscatter profiles in cirrus clouds by using a combined Raman elastic-backscatter lidar. *Appl. Opt.* **31**, 7113–7131.

Ansmann A., Bösenberg, J., Chaikovsky, A., Comeron, A., Eckhardt, S. and co-authors. 2003. Long-range transport of Saharan dust to

northern Europe: the 11-16 October 2001 ourtbreak observed with EARLINET. *J. Geophys. Res.* **108**, doi:101029/2003JD003757.

Ansmann A., Tesche, M., Knipperts, P., Bierwirth, E., Althausen, D. and co-authors. 2008. Vertical profiling of convective dust plumes in southern Morocco during SAMUM. *Tellus* **61B**, doi:10.1111/j.1600-0889.2008.00384.x.

Balis, D. S., Amiridis, V., Nickovic, S., Papayannis, A. and Zerefos, C. 2004. Optical properties of Saharan dust layers as detected by a Raman lidar at Thessaloniki, Greece. *Geoph. Res. Lett.* **31**, 13104, doi:10.1029/2004GL019881.

Bierwirth, E., Wendisch, M., Ehrlich, A., Heese, B., Tesche, M. and co-authors. 2008. Spectral surface albedo over Morocco and its impact on the radiative forcing of Saharan dust. *Tellus* **61B**, doi:10.1111/j.1600-0889.2008.00395.x.

Cairo, F., Donfrancesco, G. D., Adriani, A., Pulvirenti, L. and Fierli, F. 1999. Comparison of various linear depolarization parameters measured by lidar. *Appl. Opt.* **38**, 4425–4432.

Chazette, P., Sanak, J. and Dulac, F. 2007. New approach for aerosol profiling with a lidar onboard an ultralight aircraft: application to the African Monsoon Multidisciplinary Analysis. *Environ. Sci. Technol.* **41**, 8335–8341, doi:10.1021/es070343y.

Draxler, R. R. and Rolph, G. D. 2003. HYSPLIT (HYbrid Single-Particle Lagrangian Integrated Trajectory), Model access via NOAA ARL READY website: http://www.arl.noaa.gov/ready/hysplit4.html, NOAA Air Resources Laboratory, Silver Spring, MD.

Esselborn, M., Wirth, M., Fix, A., Weinzierl, B., Rasp, K. and co-authors. 2008. Spatial distribution and optical properties of Saharan dust observed by airborne high spectral resolution lidar during SAMUM 2006. *Tellus* **61B**, doi:10.1111/j.1600-0889.2008.00394.x.

Fernald, F. G. 1984. Analysis of atmospheric lidar observations. *Appl. Opt.* **23**, 652–653.

Freudenthaler, V., Esselborn, M., Wiegner, M., Heese, B., Tesche M. and co-authors. 2008. Depolarization-ratio profiling at several wavelengths in pure Saharan dust during SAMUM 2006. *Tellus* **61B**, doi:10.1111/j.1600-0889.2008.00396.x.

Gibert, F., Cuesta, J., Yano, J.-I., Arnault, N. and Flamant, P. H. 2007. On the correlation between convective plume updrafts and downdrafts, lidar reflectivity and depolarization ratio. *Boundary-Layer Meteorol.* **125**, 553–573, doi:10.1007/s10546-007-9205-6.

Hamonou, E., Chazette, P., Balis, D., Dulac, F., Schneider, X. and co-authors. 1999. Characterization of the vertical structure of Saharan dust export to the Mediterranean basin. *J. Geophys. Res.* **104**, 22 257–22 270.

Haywood, J. M., Francis, P., Osborne, S. R., Glew, M., Loeb, N. and co-authors. 2003. Radiative properties and direct radiative effect of Saharan dust measured by the C-130 aircraft during SHADE: 1. Solar spectrum. *J. Geophys. Res.* **108**, 8577, doi:10.1029/2002JD002687.

Heese, B. and Wiegner, M. 2008. Vertical aerosol profiles from Raman-polarization lidar observations during the dry season AMMA field campaign. *J. Geophys. Res.* **113**, D00C11, doi:10.1029/2007JD009487.

Heese, B., Freudenthaler, V., Seefeldner, M. and Wiegner, M. 2002. POLIS—A new POrtable LIdar System for ground-based and airborne measurements of aerosols and clouds. In: *Lidar Remote Sensing in Atmospheric and Earth Sciences* (eds. L. R. Bissonnette, G. Roy and G. Vallee). Defence Research and Development, Canada–Valcartier, Val–Belair, Quebec, Canada, 71–74.

Heese, B., Freudenthaler, V., Seefeldner, M., Kosmale, M. and Wiegner, M. 2004. First results from the portable lidar system POLIS. In: *Proceedings of the International Laser Radar Conference*, Matera, Italy, ESA SP-561, 79–82.

Heintzenberg, J. 2008. The SAMUM-1 experiment over Southern Morocco: overview and introduction. *Tellus* **61B**, doi:10.1111/j.1600-0889.2008.00403.x.

Holben, B. N., Tanré, D., Smirnov, A., Eck, T. F., Slutsker, I. and co-authors. 2001. An emerging ground-based aerosol climatology: aerosol optical depth from AERONET. *J. Geophys. Res.* **106**, 12 067–12 097.

von Hoyningen-Huene, W. and Posse, P. 1997. Non-sphericity of aerosol particles and their contribution to radiative forcing. *J. Quant. Spectrosc. Rad. Trans.* **57**, 651–668.

von Hoyningen-Huene, W., Dinterfnm T., Kokhanovsky, A. A., Burrows, J. P. and Diouri, M. 2008. Measurements of desert dust optical characteristic at Porte au Sahara during SAMUM. *Tellus* **61B**, doi:10.1111/j.1600-0889.2008.00405.x.

Johnson, B. T., Heese, B., Mc Farlane, S., Chazette, P., Jones, A. and co-authors. 2008. Vertical distribution and radiative effects of mineral dust and biomass burning arosol over West Africa during DABEX. *J. Geophys. Res.* **113**, D00C12, doi:10.1029/2008JD009848.

Kahn, R., Petzold, A., Wendisch, M., Bierwirth, E., Dinter, T. and co-authors. 2008. Desert dust aerosol air mass mapping in the western Sahara, using particle properties derived from space-based multi-angle imaging. *Tellus* **61B**, doi:10.1111/j.1600-0889.2008.00398.x.

Kandler, K., Schütz, L., Deutscher, C., Ebert, M., Hofmann, H. and co-authors. 2008. Size distribution, mass concentration, chemical and mineralogical composition, and derived optical parameters of the boundary layer aerosol at Tinfou, Morocco, during SAMUM 2006. *Tellus* **61B**, doi:10.1111/j.1600-0889.2008.00385.x.

Knippertz, P., Ansmann, A., Althausen, D., Müller, D., Tesche, M. and co-authors. 2008. Dust mobilization and transport in the Northern Sahara during SAMUM 2006 – A meteorological overview. *Tellus* **61B**, doi:10.1111/j.1600-0889.2008.00380.x.

Léon, J.-F., Tanré, D., Pelon, J., Kaufman, Y. J., Haywood, J. M. and co-authors. 2003. Profiling of a Saharan dust outbreak based on a synergy between active and passive remote sensing. *J. Geophys. Res.* **108**, doi:10.1029/2002JD002774, 8575.

Mattis, I., Ansmann, A., Müller, D., Wandinger, U. and Althausen, D. 2002. Dual-wavelength Raman lidar observations of the extinction-to-backscatter ratio of Saharan dust. *Geoph. Res. Lett.* **29**, 1306, doi:10.1029/2002GL014721.

Müller, D., Ansmann, A., Mattis, I., Tesche, M., Wandinger, U. and co-authors. 2007. Aerosol-type-dependent lidar ratios observed with Raman lidar. *J. Geophys. Res.* **112**, doi:10.1029/2006JD008292.

Murayama T., Okamoto, H., Kaneyasu, N., Kamataki, H. and Miura, K. 1999. Application of lidar depolarization measurement in the atmospheric boundary layer: effects of dust and sea-salt particles. *J. Geophys. Res.* **104**, 781–792.

Osborne, S. R., Johnson, B. T., Haywood, J. M., Baran, A. J., Harrison, M. A. J. and co-authors. 2008. Physical and optical properties of mineral dust aerosol during the Dust and Biomass-burning Experiment. *J. Geophys. Res.* **113**, D00C03, doi:10.1029/2007JD009551.

Pelon, J., Mallet, M., Mariscal, A., Goloub, P., Tanré, D. and co-authors. 2008. MICROLIDAR observations of biomass burning aerosol (Benin) during AMMA-SOP 0/DABEX. *J. Geophys. Res.* **113**, doi:10.1029/2008JD009976.

Platt, C. M. R. 1978. Lidar backscattering from horizontally oriented ice crystal plates. *J. Appl. Meteorol.* **17**, 482–488.

Prospero, J. M. 1999. Long-term measurements of the transport of African mineral dust to the southeastern United States: implications for regional air quality. *J. Geophys. Res.* **104**, 15 917–15 927.

Prospero, J. M. and Carlson, T. N. 1972. Vertical and areal distribution of Saharan dust over the western equatorial North Atlantic Ocean. *J. Geophys. Res.* **77**, 5255–5265.

Prospero, J. M., Glaccum, R. A. and Nees, R. T. 1981. Atmospheric transport of soil dust from Africa to South America. *Nature* **289**, 570–572.

Redelsperger, J.-L., Thorncroft, C. D., Diedhiou, A., Lebel, T., Parker, D. J. and co-authors. 2006. African Monsoon Multidisciplinary Analysis: an International Research Project and Field Campaign. *Bull. Am. Meteorol. Soc*. **87**, 1739–1746.

Reid, J. S., Kinney, J. E., Westphal, D. L., Holben, B. N., Welton, E. J. and co-authors. 2003. Analysis of measurements of Saharan dust by airborne and ground-based remote sensing methods during the Puerto Rico Dust Experiment (PRIDE). *J. Geophys. Res.* **108**, doi:10.1029/2002JD002493, 8586.

Sokolik, I. N., Winker, D. M., Bergametti, G., Gillette, D. A. and co-authors. 2001. Introduction to special section: outstanding problems in quantifying the radiative impacts of mineral dust. *J. Geophys. Res.* **106**, 18 015–18 028.

Tanré, D., Haywood, J. M., Pelon, J., Léon, J. F., Chatenet, B. and co-authors. 2003. Measurement and modeling of the Saharan dust radiative impact: overview of the SaHAran Dust Experiment (SHADE). *J. Geophys. Res.* **108**, 8574, doi:10.1029/2002JD003273.

Tesche, M., Ansmann, A., Müller, D., Althausen, D., Heese, B. and co-authors. 2008. Vertical profiling of Saharan dust with Raman lidars and airborne high-spectral-resolution lidar during SAMUM. *Tellus* **61B**, doi:10.1111/j.1600-0889.2008.00390.x.

Wendisch, M. and von Hoyningen-Huene, W. 1994. Possibility of refractive index determination of atmospheric aerosol particles by ground-based solar extinction and scattering measurements. *Atmos. Environ.* **28**, 785–795.